Enhanced syngas production from glycerol dry reforming over Ru promoted -Ni catalyst supported on extracted Al$_2$O$_3$

Nurul Asmawati Roslan [a], Sumaiya Zainal Abidin [b,c,*], Osarieme Uyi Osazuwa [b,d], Sim Yee Chin [a,b], Y.H. Taufiq-Yap [e,f]

[a] Department of Chemical Engineering, College of Engineering, Universiti Malaysia Pahang, Lebuhraya Tun Razak, 26300, Gambang, Kuantan, Pahang, Malaysia
[b] Centre for Research in Advanced Fluid & Processes (FLUID CENTRE), Universiti Malaysia Pahang, 26300 Gambang, Kuantan, Pahang, Malaysia
[c] Faculty of Chemical Engineering, Industrial University of Ho Chi Minh City, 12 Nguyen Van Bao St, Go Vap, Ho Chi Minh City 7000, Vietnam
[d] Department of Chemical Engineering, University of Benin, PMB 1154, Benin City, Edo State, Nigeria
[e] Catalysis Science and Technology Research Centre (PutraCAT), Faculty of Science, Universiti Putra Malaysia, 43400, UPM, Serdang, Selangor, Malaysia
[f] Chancellery Office, Universiti Malaysia Sabah, 88400, Kota Kinabalu, Sabah, Malaysia

ARTICLE INFO

ABSTRACT

Crude glycerol, a by-product of biodiesel production, has drawn considerable attention to the importance of glycerol valorization through dry reforming reaction to obtain syngas. The selection of suitable catalysts is significantly important to enhance the catalytic activity in glycerol dry reforming (GDR) reactions. Hence, Ru with different loadings (i.e. 1%, 2%, 3%, 4%, 5%) doped in 15% Ni-extracted Al$_2$O$_3$(EA) was evaluated as catalyst via GDR process in this study. The catalyst prepared by ultrasonic-impregnation assisted technique was subjected to 8 h of CO$_2$ reforming of glycerol. The reactant conversions and products yield was in the order of 3% Ru-15%Ni/EA > 5%Ru-15%Ni/EA > 4%Ru-15%Ni/EA > 2%Ru-15%Ni/EA > 1%Ru-15%Ni/EA > 15%Ni/EA, while the quantity of carbon deposited was in the order 15%Ni/EA > 1%Ru-15%Ni/EA > 2%Ru-15%Ni/EA > 4%Ru-15%Ni/EA > 5%Ru-15%Ni/EA > 3%Ru-15%Ni/EA. 3%Ru-15%Ni/EA attained the greatest glycerol conversions of 90%, H$_2$ yield of 80% and CO yield of 72% with the lowest carbon deposition of 7.38%. The dispersion of Ni particles on EA support evidently improved after the promotion step with Ru, which minimized the agglomeration of Ni and smaller crystallite size. In addition, the introduction of Ru increased the oxygen storage capacity which significantly reduced the formation of carbon during the reaction. GDR's optimal reaction temperature obtained over 3%Ru-15%Ni/EA catalysts was at 1073 K (i.e. 93% glycerol conversion; 87% H$_2$ yield; 79% CO yield). Over a 72 h time on stream at 1073 K, 3%Ru-15%Ni/EA catalyst had superior catalytic activity and stability. Overall, 3%Ru-15%Ni/EA catalyst was more coke-resistant than other promoted catalysts due to its accessible structure, higher oxygen storage capacity, moderate basicity, uniformly dispersed Ni phase and stronger Ru/Ni-EA interaction.

1. Introduction

Nowadays, the high usage of non-renewable fuel sources (i.e. natural gas, petroleum, and coal) has lead to the oil reserves depletion and global warming effects [1,2]. A significant efforts have been taken to mitigate these related problems by replacing these sources with syngas (i.e. mixture of H$_2$ and CO).

Currently, glycerol dry reforming (GDR) reaction has gained significant attention due to the reaction's ability to convert a greenhouse gaseous (CO$_2$) and biodiesel by-product (glycerol) into valuable product like syngas [3–5]. Syngas with molar ratio less than two has been

successfully produced by the reaction, which is suitable for Fischer-Tropsch (FT) production. [5]. Despite those mentioned advantages, deactivation of catalyst triggered by carbon deposition and active metals sintering are the major problems in GDR reaction [6,7]. As a result of these drawbacks, research in this area has been directed toward the development of effective catalysts that can improve catalytic performance while also minimizing carbon entrapment.

Nickel (Ni)-based catalysts have been widely used in the reforming process. It has been demonstrated that Ni has a significant impact on the syngas generation process by enhancing water gas shift (WGS) reactions and the reproduction of syngas. [8]. Besides that, this type of catalyst

can effectively break C–H and C–C bonds [7,9,10]. Additionally, Ni-based catalysts have been widely used due to its high activity, wide-range application and low-cost [11–13]. However, due to poor thermal stability, Ni-based catalyst is easily deactivated during the reaction. At elevated reaction temperatures (>1073 K), metal sintering occurs easily, impeding the reforming reaction and catalytic activity [14,15]. The stability and activity of supported Ni-based catalysts have previously been reported to be enhanced by altering the catalyst's synthesis process and surface modification with promoters [15].

The utilization of noble metals as a promoter in reforming processess such as Ir, Ru, Rh, Pt and Pd [16–18] has been widely evaluated due to their effectiveness in enhancing the stability, catalytic activity and excellent resistance against carbon deactivation. De Caprariis et al. [19] investigated the utilization of different active metals such as Ru, Rh and Pt in producing perovskite-type oxide catalysts. All catalysts were capable of achieving high reactant conversions (>80%), and interestingly, both Rh and Ru catalysts demonstrated negligible catalyst deactivation after 65 h of reforming, thereby proving the catalyst's high stability. Among these noble metals, Ru is preferred due to its high stability and display of high catalytic activity [20–22]. In addition, the implementation of Ru as dopants over Ni catalysts has gained much interest due to its ability to suppress carbon formation. Recently, the use of Ru as a promoter has piqued researchers' interest in reducing carbon formation and improving catalyst stability; however, using Ru alone is not cost effective. Furthermore, while the catalytic activity of Ru as a mono-metallic catalyst is lower than that of Ni, the addition of Ru to the Ni-based catalyst as a promoter increases the reducibility of Ni and inhibits deactivation [23–26]. Thus, the addition of Ru noble metal as catalyst promoter could be a better option to enhance the catalytic activity and inhibit the carbon formation. Even though Ru has demonstrated a great physicochemical properties and catalytic performance in reforming processes, the influence of Ru as a promoter over Ni-based catalysts in GDR has not been explored. According to Nisa et al. [27], the performance of Ru can be improved by using basic support with good redox properties. Basic supports are able to provide anionic species (i.e. OH or O) that can spread onto the Ru surface and oxidize the carbon species during the reaction. In addition, tuning the support property can change the activities of both Ni and Ru [28].

Previously, it has been proven that the catalyst's supports such as Al_2O_3, MgO and SiO have a great capability to enhance the active metal dispersion and improve thermal stability of the catalyst [19]. Among these, Al_2O_3 has been widely used due to the high surface area, ability to inhibit catalyst sintering, and good metal dispersion [29–32]. Besides, Al_2O_3 is able to ensure the synthesized catalyst was thermally stable even at high reaction temperature [33]. Recently, Li et al. [34] investigated the advantages of the confinement effect owned by support towards bi-metallic catalysts (i.e. Ni-Fe). Ni-Fe catalyst with Fe-loading < 0.7 wt% showed a stable catalytic activity in 24 h reaction time with low carbon deposition and no apparent sintering of active metal. In addition, the confinement effect of these supports effectively reduced the sintering of metal, which could lead to the catalyst's deactivation [34,35]. Though, there is a limited number of researches that are focused on the employment of catalyst support in GDR from industrial waste. Lee et al. [36] investigated the incorporation of Ni onto the cement clinker support in GDR reaction. High reactant conversion ranging from 70 − 80% at a CGR of 1–1.67 was observed. Recently, our research team has conducted a study on the utilization of extracted Al_2O_3 (EA) from aluminum dross (AD) as a catalyst support in GDR reaction [37]. Besides having a high specific surface area and enhancing the Ni dispersion, EA contributed in reducing the carbon formation during the reaction.

To the best of our knowledge, the combination of EA as a catalyst support and Ru's utilization as a promoter in GDR reaction has not been reported previously. Therefore, the impact of Ru promoter towards the physicochemical properties of Ni/EA catalyst was evaluated in this study. In addition, the correlations between catalytic activity and physicochemical properties of Ru-Ni/EA catalyst in GDR are elucidated,

and the effect of promoter loading and reaction temperature was also investigated. Finally, catalysts' stability was evaluated in a continuous dry reforming reaction for 72 h.

2. Experimental procedure

2.1. Support preparation

The acid leaching approach was employed for the preparation of Al_2O_3 from AD. This method was adopted and modified from a study by How et al. [38] and Roslan et al. [37]. In this study, AD was collected from one of the waste collection centre in Malaysia. Firstly, AD was washed several times with distilled water to eliminate the chloride content. The chloride content in the remaining solution was tested using Mohr's method, and the process was repeated 3–4 times until all the chloride content was eliminated. Then, in a 500 mL beaker containing 50 g of washed dross, 200 mL of sulphuric acid was added, and the solution was continuously stirred (400 rpm) and heated (343 K) for 2 h and left to settle for 12 h. Two-layer solution was obtained which consist of a clear solution at the top and solid residue at the bottom. To collect the clear solution, the solid residue was filtered. Leftover insoluble particle was removed and the filtrate (i.e., clear solution) was used in the co-precipitation process. In this stage, 10 % ammonia solution was added dropwise to obtain a solution with pH of 6.0. Then, ultrasonication was introduced into the resulting solution for 15 min. The product obtained was centrifuged for 20 min and washed with deionized water until pH 7.0 solution was obtained. Finally, the sample was air-dried overnight at 383 K and air-calcined for 6 h at 873 K. The extracted product was denoted as EA.

2.2. Catalyst preparation and characterizations

1%Ru-15%Ni/EA and 15%Ni/EA catalysts were prepared by ultrasonic-impregnation assisted technique. 15%Ni/EA was first prepared by adding nickel (II) nitrate hexahydrate (Merck, 99%) solution into a beaker containing EA. The solution was placed in an ultra-sonication water bath at 353 K for 4 h. The collected particles were air-dried for 12 h at 383 K followed by the calcination process for 5 h at 1223 K. After that, 1 wt% of ruthenium (III) chloride hydrate (Sigma Aldrich, 99.98%) was prepared by adding Ru solution into a beaker containing 15%Ni/EA particles and placed under ultrasonic irradiation for 4 h. These collected powders were air-dried in an oven for 12 h at 383 K and calcined at 823 K. The same technique was used to synthesize X%Ru-15%Ni/EA (X = 1,2,3,4,5). All synthesized catalysts were characterized by X-ray diffraction (XRD), H_2-temperature-programmed reduction (H_2-TPR), CO_2-temperature programmed desorption (CO_2-TPD) and N_2 physisorption analyses. Meanwhile, the used catalysts were characterized by X-ray photoelectron spectra (XPS), transmission electron microscopy (TEM) and temperature-programmed oxidation (TPO).

2.2.1. X-ray diffraction (XRD)

To analyze the crystal structure of the EA, fresh and used catalysts, XRD were performed using Rigaku Miniflex II instrument. The analysis employs the Cu monochromatic anode as a source of X-ray radiation with a wavelength of $\lambda = 1.5418$ Å at 30 kV and 15 mA. XRD patterns were examined within 2θ range of 10°- 80° with low scan speed of 1° per min and stride size of 0.02°.

2.2.2. H_2 temperature programmed reduction (H_2-TPR)

H_2-TPR measurement was carried out using Micromeritics AutoChem II-2920 chemisorption unit to evaluate the reducibility of the synthesized catalysts. In this study, 0.1 g of catalyst sample was initially treated under a He gas flow (50 mL min^{-1}) for 30 min at 373 K to eliminate any moisture and volatile compounds. Then, the H_2 reduction process was conducted. The sample was exposed to 50 mL min^{-1} of gas mixture (10%H_2/Ar) from 373 to 1173 K with a heating rate of 10 K

min^{-1}. The reduction temperature was maintained at 1173 K for 30 mins before the samples are cooled down to complete the reduction process. Thermal conductivity detector (TCD) was used to determine the hydrogen consumption, while the amount of H$_2$ uptake in the reduction process was estimated by integrating H$_2$-TPR profiles.

2.2.3. CO$_2$-temperature programmed desorption (CO$_2$-TPD)

The basicity of the catalysts was computed using CO$_2$-TPD, carried out on a TP-5000 system. 50 mg of sample was loaded in a quartz reactor and treated using He flows at 473 K for 30 min. Then, the sample was degassed over CO$_2$ for 1 h and purged with helium to remove the adsorbed CO$_2$. Finally, the sample was heated from room temperature to 1173 K at a ramping rate of 10 K min^{-1} and CO$_2$-TPD was monitored using a TCD.

2.2.4. X-ray photoelectron spectra (XPS)

XPS was conducted to study the chemical state and elemental composition of the used catalysts using ULVAC-PHI 500 (Versa Probe II). The analysis was conducted using multi-channel detector with analyzer pass energy of 10 eV and energy resolution of < 0.65 eV. The narrow spectra obtained from XPS measurement was interpreted using CasaXPS Version 2.3.16 and calibrated using the peak energy of adventitious carbon at 284.5 eV.

2.2.5. Transmission electron microscopy (TEM)

TEM analysis was performed to study the surface morphology of the used catalyst. The images were captured using a Philips CM 12 (Netherlands) transmission electron microscope with a tension voltage of 120 kV. The powder sample was suspended in 100% ethanol under an ultrasonic process for 30 mins. After that, a drop of the solution was taken and placed on the TEM copper grid. The sample was then dried for 5 mins before being viewed under the TEM microscope for analysis.

2.2.6. Temperature-programmed oxidation (TPO)

TPO analysis is a common method to evaluate the nature of carbonaceous species accumulated on the used catalyst surface. This analysis was performed on the used catalyst using a TGA Q500 (TA Instruments). For complete removal of moisture and volatile compounds, a sample was initially preheated at 373 K with a 10 K min^{-1} heating rate for 30 mins in N$_2$ flow at 100 mL min^{-1}. Then, the temperature was raised to 1023 K with different heating rates of 10, 15, and 20 K min^{-1} in the gas mixture of 1O$_2$: 4 N$_2$ (100 mL min^{-1}) for 30 mins and kept isothermally. Subsequently, the sample was cooled down at room temperature in the same gas mixture. The obtained results showed the weight changes versus temperature profile.

2.3. GDR evaluation

The performance of 15%Ni/EA and X%Ru-15%Ni/EA in GDR reaction was evaluated for 8 h under atmospheric pressure. About 0.2 g of catalyst was inserted inside the fixed bed reactor. Before the reaction, a mixture of 50% N$_2$ and 50% H$_2$ gas was fed into the reactor for the in-situ catalyst reduction (50 mL min^{-1}) at 973 K. After 1 h, CO$_2$ gas and glycerol were fed into the reactor with a 120 mL min^{-1} of total flow rate. To regulate the inlet gaseous flowrate, a mass flowmeter controller was located at the reactor. Meanwhile, to allow only gaseous products flow into the effluent stream, a water-trap was built in the system. The collected products was then analyzed using TCD gas chromatograph. To evaluate the catalytic performance in GDR reaction, values of reactant conversion, products yield and H$_2$:CO ratio were calculated based on Eqs. (1)–(5).

Conversion of glycerol to gaseous product:

$$X_G = \frac{2F_{H_2} \times 4F_{CH_4}}{8F_{C_3H_8O_3}} \times 100 \tag{1}$$

The yield of carbon-containing species:
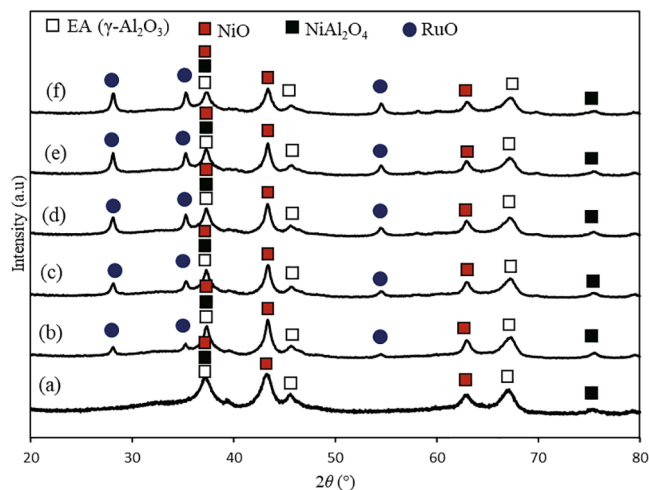
Fig. 1. X-ray diffractograms of (a) 15%Ni/EA, (b) 1%Ru-15%Ni/EA, (c) 2%Ru-15%Ni/EA, (d) 3%Ru-15%Ni/EA, (e) 4%Ru-15%Ni/EA, (f) 5%Ru-15%Ni/EA.

$$Y_i = \frac{F_i}{3 \times F_{C_3H_8O_3}} \times 100 \tag{2}$$

Where, i= CH$_4$, CO$_2$ and CO; F_i= molar flow rate of component i (mol s^{-1})

Hydrogen yield:

$$Y_{H_2} = \frac{2F_{H_2}}{8F_{C_3H_8O_3}} \times 100 \tag{3}$$

Reaction rate of products formation:

$$r_i\left(mol g_{cat}^{-1} s^{-1}\right) = \frac{y_i \times F_{i,outlet}}{W} \tag{4}$$

where, i= H$_2$, CH$_4$, CO$_2$ and CO; y_i= dry basis composition of product i; $F_{i,outlet}$ = molar flow rate of component i (mol s^{-1}); W= weight of catalyst (g)

Product ratio:

$$R_{i/j} = \frac{r_i}{r_j} \tag{5}$$

where, r= product formation rate; i = H$_2$; j = CO

3. Results and discussions

3.1. Characterization of the catalyst

Fig. 1 depicts the X-ray diffractograms of all the synthesized catalysts including the unpromoted (i.e. 15%Ni/EA) catalyst. All the synthesized catalysts displayed phase reflection of γ-Al$_2$O$_3$ at 2θ = 19.8°, 32.9°, 36.4°, 39.1°, 45.9°, 60.8°, and 67.3° (JCPDS No: 00–029-0063), which matched with the spectrum of γ-Al$_2$O$_3$ support as reported by Yin et al [39]. In addition, the NiO crystalline spectrum was observed at 2θ = 37.4°, 43.5° and 63.3° (JCPDS card No: 01–073-1519) for all unpromoted and promoted catalysts. The promoted and unpromoted catalysts also exhibited the characteristic peaks of spinel NiAl$_2$O$_4$ at 2θ = 37.4° and 75.5° (JCPDS No: 00–010-0339) as illustrated in Fig. 1(b) - (f), which indicates strong Ni-EA interaction. It is noteworthy that all the promoted catalysts (i.e. 1%Ru-15%Ni/EA, 2%Ru-15%Ni/EA, 3%Ru-15%Ni/EA, 4%Ru-15%Ni/EA and 5%Ru-15%Ni/EA) displayed diffraction line of RuO at 2θ = 28.37°, 35.57° and 54.82° (JCDPS card No: 01–088-0322). The presence of RuO elements indicates that the Ru particles were effectively dispersed on the 15%Ni/EA catalyst.

The crystallite size of the unpromoted and promoted catalysts were calculated using Scherer equation at XRD peak of 2θ = 43.5° and

Table 1
Physical properties of EA, 1%Ru-15%Ni/EA, 2% Ru-15%Ni/EA, 3% Ru-15%Ni/EA, 4%Ru-15%Ni/EA and 5%Ru-15% Ni/EA.

Catalyst	BET surface area ($m^2 g^{-1}$)	Average pore volume ($cm^3 g^{-1}$)	Average pore diameter (nm)	Average NiO particle size (nm)		Deactivation degree, D_d (%)
				Fresh[a]	Used[b]	
EA	267.53	0.85	16.2	–	–	–
15%Ni/EA	165.36	0.64	18.3	5.67	6.23	3.45
1%Ru-15%Ni/EA	148.81	0.60	17.6	5.32	6.12	0.63
2%Ru-15%Ni/EA	136.16	0.58	16.9	5.29	5.42	2.29
3%Ru-15%Ni/EA	125.32	0.57	16.5	5.23	5.36	0.56
4%Ru-15%Ni/EA	119.91	0.55	16.3	5.25	5.41	0.57
5%Ru-15%Ni/EA	108.32	0.53	15.8	5.27	5.42	2.60

[a]The crystallite size of the synthesized catalyst was calculated using XRD analysis.
[c]Deactivation degree, D_d (%)= $(X_{1h} - X_{8h})/X_{1h} \times 100$ where X is conversion value of glycerol.
[b] The average crystallite size was calculated using TEM analysis.

summarized in Table 1. The NiO crystallite size for 15%Ni/EA was 5.67 nm and after the addition of promoter, the value of catalyst's crystallite size was reduced in the following order: 15%Ni/EA (5.67 nm) > 1%Ru-15%Ni/EA (5.32 nm) > 2%Ru-15%Ni/EA (5.29 nm) > 5%Ru-15%Ni/EA (5.27 nm) > 4%Ru-15%Ni/EA (5.25 nm) > 3%Ru-15%Ni/EA (5.23 nm). This can be attributed to the improvement in dispersion of NiO particles with the presence of Ru promoter. Indeed, Paviotti et al. [40] and Hossain et al. [41] observed a similar trend in the size of Ni crystallites after promoter was added to synthesized catalysts. Both studies discovered that incorporating a promoter improved the interaction between metal and support by preventing metal particle agglomeration on the catalyst surface.

Table 1 presents the physical characteristics of the synthesized support and catalysts. From the table, a reduction in the BET surface area and pore volume was found in the order; EA support > Ni/EA > 15%Ni/

EA > 1%Ru-15%Ni/EA > 2%Ru-15%Ni/EA > 3%Ru-15%Ni/EA > 4%Ru-15%Ni/EA > 5%Ru-15%Ni/EA. This pattern is attributed to the pore structure of the EA support and the presence of NiO on the catalyst's surface. Interestingly, the pore diameter was slightly increased upon addition of Ni into the EA support which implied agglomeration of Ni in the pore, leading to pore expansion. However, the addition of promoter onto the 15%Ni/EA catalyst reduced the catalyst's pore diameter. This demonstrates a uniform distribution of Ni metal across the surface and pores of the EA support. Based on IUPAC sorption isotherms, all the synthesized catalysts showed type H2 hysteresis loop from type IV curve. This type of isotherm represents the mesoporosity of the synthesized material. In addition, H2 type hysteresis loop suggests that mesoporous particles undergoes a capillary condensation phenomenon [42].

Fig. 2 (a). illustrates the H_2-TPR profile of 1%Ru-15%Ni/EA, 2%Ru-15%Ni/EA, 3%Ru-15%Ni/EA, 4%Ru-15%Ni/EA and 5%Ru-15%Ni/EA
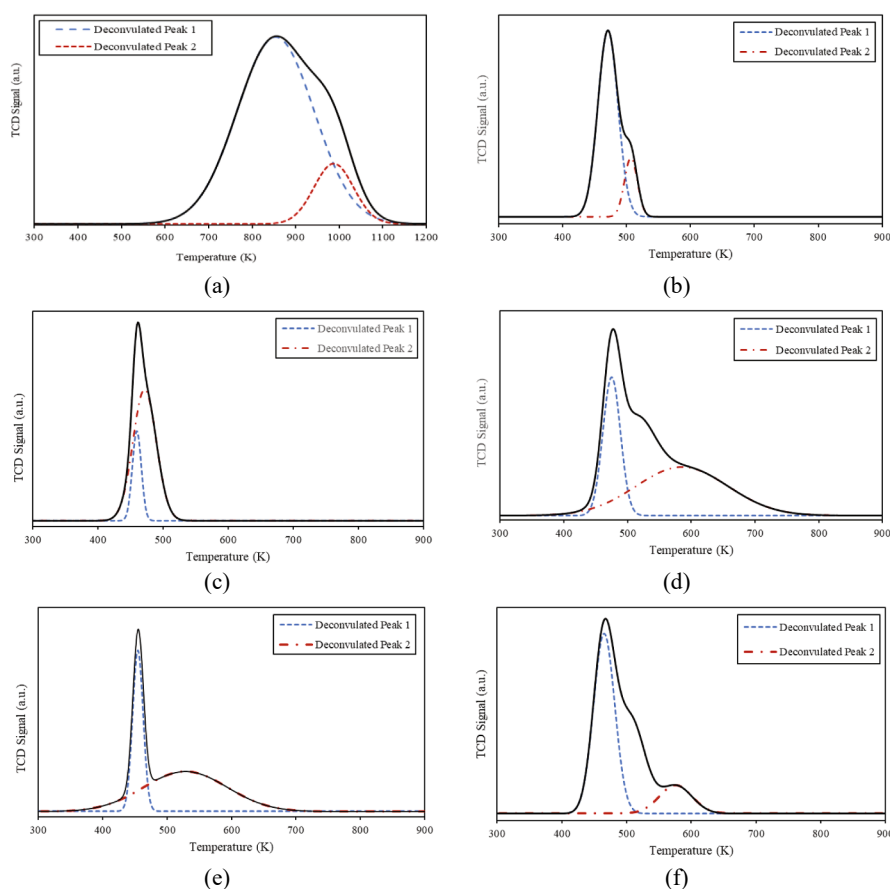
Fig. 2. H_2-TPR profile of 15%Ni/EA, 1%Ru-15%Ni/EA, 2% Ru-15%Ni/EA, 3%Ru-15% Ni/EA, 4%Ru-15%Ni/EA and 5%Ru-15%Ni/EA.
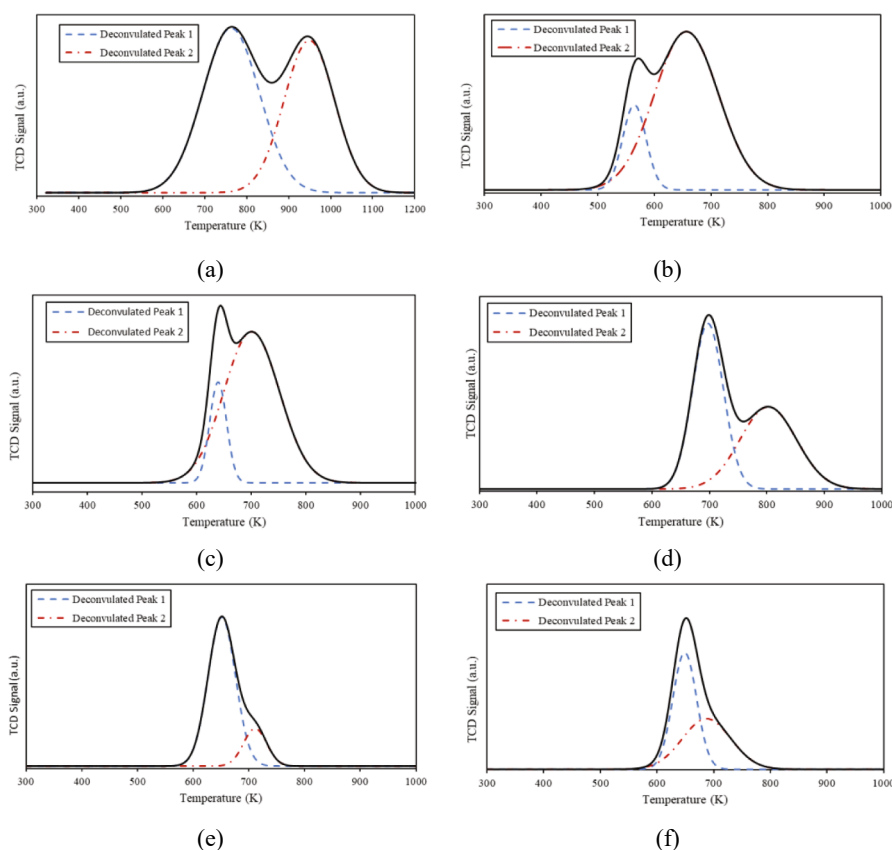
Fig. 3. CO_2-TPD of (a) 15%Ni/EA, (b) 1%Ru-15% Ni/EA, (c) 2%Ru-15%Ni/EA, (d) 3%Ru-15%Ni/EA, (e) 4%Ru-15%Ni/EA, (f) 5%Ru-15%Ni/EA.

catalysts. Peak appeared for 15%Ni/EA at temperature range of 573 K–1151 K representing the reduction of NiO species to Ni° metallic phase with weak interaction between support and metal [43,44]. The second peak located at a reduction temperature of 833–1151 K was due to the NiO particles reduction located in the bulk EA support with a strong metal-support interaction (i.e., Eq. (6)).

$$NiO + H_2 = Ni + H_2O \qquad (6)$$

Peak appearing at reduction temperature > 923 K represents the reduction of $NiAl_2O_4$ spinel structure, which is probably due to the high diffusion of Ni into the EA support [45,46]. The incorporation of Ru promoter over 15%Ni/EA catalyst shifted the peaks towards lower reduction temperature (<800 K) as against the peak for the 15%Ni/EA catalyst. This demonstrates the effect of a second metal, Ru, on the NiO particle reduction point due to the spillover of H_2 dissociated on NiO and Ru [47]. The addition of Ru also enhance the level of surface oxygen mobility, hence, lowering the reduction ability of Ni [48]. The decrease in reduction temperature is due to the presence of the Ru promoter, which restricts the migration of Ni ions into the EA support structure while also reducing the Ni-Al_2O_3 interaction. Hossain et al. [48] reported a similar trend whereby the reduction peak of Ni shifted to a lower point after the addition of promoter into Ni/Al_2O_3 catalyst. From Fig. 2(b), all the prepared promoted catalysts exhibited two main deconvoluted reduction peaks. The main peak depicts the reduction of RuO_2 to metallic Ru [49,50,51]. From the deconvulated peaks, the low temperature reduction peaks (i.e. 400–470 K) can be ascribed to the reduction of well dispersed RuO_2 species. Meanwhile, higher reduction temperature peaks (i.e. 490–800 K) can be attributed to the reduction of oxidized Ru [52] or Ru dissolution in the spinel lattice, as suggested by Bossola et al. [51]. Additionally, higher reduction temperature suggests good stabilization of oxidized Ru in the catalyst matrix. The peak of the promoted catalysts shifts to a higher temperature from 1%Ru-15%Ni/

EA to 3%Ru-15%Ni/EA catalysts. This indicates a strong interaction of the support and active phase. Based on the H_2-TPR profile presented in Fig. 2, as the loading of Ru increased, the reduction temperature shifts to a higher reduction temperature region, indicating a strong interaction between metal and support [53]. The higher metal-support interaction was most likely caused by the uniform dispersion of smaller NiO crystallite sizes on the surface of the EA support, which resulted in higher metal-support interaction [54]. However, at 4%Ru-15%Ni/EA and 5% Ru-15%Ni/EA, the reduction was slightly reduced. At 3% there is sufficient Ru molecule available to create the required metal to metal bond which is needed to interact with the support at the molecular level. That is at below or above 3% the Ru molecules are insufficient or in excess of the required amount needed to create the ideal metal-support interaction which would enhance the catalytic performance during reaction. Hence, it can be concluded that Ru significantly affected the reducibility of the Ni species in the synthesized catalysts.

Fig. 3 represents CO_2-TPD profile of 15%Ni/EA, 1%Ru-1% Ni/EA, 2%Ru-15%Ni/EA, 3%Ru-15%Ni/EA, 4%Ru-15%Ni/EA and 5%Ru-15% Ni/EA. Two distinct peaks were observed for the 15% Ni/EA at temperature ranged 533–1000 K and 739–1177 K representing medium and strong basic sites. Meanwhile, two peaks were visible for all promoted catalysts at 531–700 K and 531–900 K. This indicates that all promoted catalysts have higher medium strength basicity to adsorb CO_2 gas. Medium basicity of all the promoted catalysts probably due to the replacement of Al ions in the brucite layers by Ru ions [55]. In this study, 3%Ru-15%Ni/EA had the highest capacity to adsorb CO_2 (129.65 μmol g^{-1}) onto its surface. High amount of CO_2 adsorbed by the catalyst suppresses the carbon formation during the reaction [36] and thus, increases the catalytic performance. The promoted catalyst's basicity was in the order of 3%Ru-15%Ni/EA > 4%Ru-15%Ni/EA > 5%Ru-15%Ni/ EA > 2%Ru-15%Ni/EA > 1%Ru-15% Ni/EA.
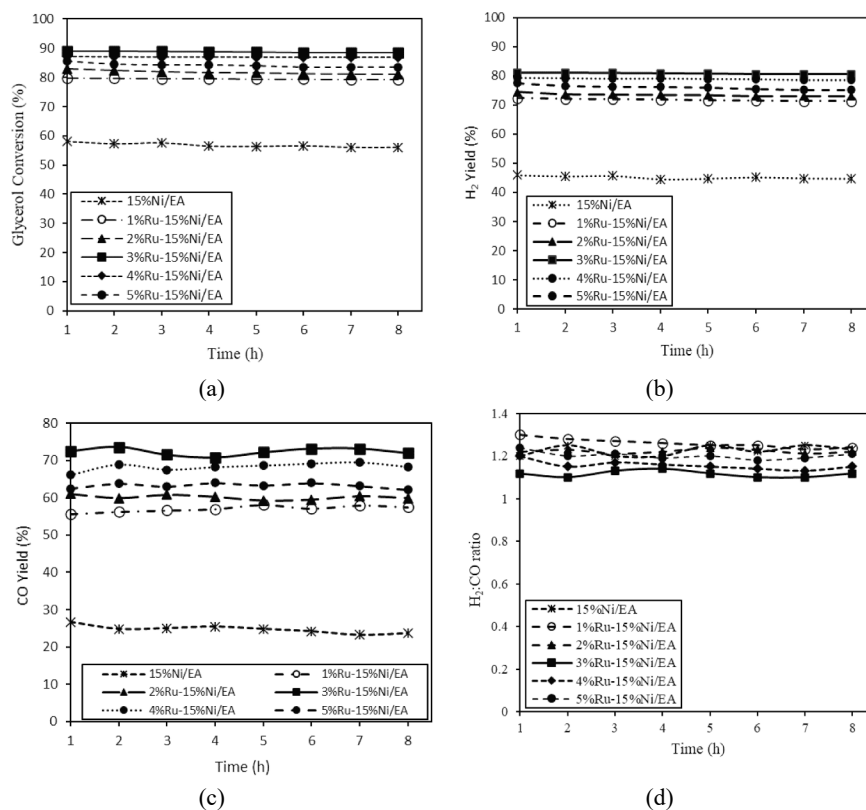
Fig. 4. Catalytic evaluation of unpromoted catalyst and promoted catalysts at various loading on; (a) glycerol conversion, (b) H$_2$ yield, (c) CO yield and (d) H$_2$: CO ratio.

3.2. Catalytic evaluation in glycerol dry reforming

3.2.1. Effect of catalyst loading

The catalytic activity of the promoted and unpromoted catalysts at 973 K for 8 h with feed ratio of CO$_2$ to glycerol (CGR) = 1 is presented in Fig. 4 (a). Metallic Ni sites showed a positive role in GDR reaction which was proven by the higher catalytic performance of 15% Ni/EA catalyst (i.e. 56% glycerol conversion, 45% H$_2$ yield and 40% CO yield) as against the EA support only (i.e. 5.2% glycerol conversion). As represented in Fig. 4, the glycerol conversion significantly increased after the adoption of Ru promoted catalyst due to the fine NiO dispersion and greater oxygen vacancies of the promoter. The reactant conversion and product yield increased in the order of 3%Ru-15%Ni/EA (90%) > 4% Ru-15%Ni/EA (86%) > 5%Ru-15%Ni/EA (84%) > 2%Ru-15%Ni/EA (81%) > 1%Ru-15%Ni/EA (79%) > 15%Ni/EA (56%). The enhancement of the Ni/EA catalysts activity via the addition of Ru promoter was consistent with literature (Paviotti et al. [40]; Hossain et al. [41]; Pauletto et al. [56]).

To investigate the stability of the catalyst, the deactivation degree of the catalyst was determined by measuring a decrease in glycerol conversion (i.e. Table 1). It was found that the degree of catalyst deactivation calculated for all synthesized catalysts were in the following order: 3%Ru-15%Ni/EA (0.55%) < 4%Ru-15%Ni/EA (0.57%) < 5%Ru-15%Ni/EA (0.63%) < 2%Ru-15%Ni/EA (2.23%) < 1%Ru-15%Ni/EA (2.60%) < 15%Ni/EA (3.45%). These findings were related to the redox properties exhibited by Ru [57]. Oh et al. [58] explored the redox properties of Ru in Ni-based catalysts for the production of syngas. According to the authors, redox properties did not only improve the stability of catalyst, but also enhanced the gasification of carbon and thereby hindering the catalyst deactivation.

Fig. 4(a) - (c) shows the overall catalytic activity of unpromoted and promoted catalyst during 8 h GDR reaction. It was found that 3%Ru-15% Ni/EA catalyst had the highest product yield (i.e. H$_2$ (80%) and CO yield

(72%)), compared to the other catalysts. As presented in Fig. 4(b) and 4 (c), the yield values were slightly improved in the order of 3%Ru-15% Ni/EA > 4%Ru-15%Ni/EA > 5%Ru-15%Ni/EA > 2%Ru-15%Ni/EA > 1%Ru-15%Ni/EA > 15%Ni/EA. As a result of these findings, it was demonstrated that the incorporation of promoter was critical in increasing the catalytic activity of GDR, which can be attributed to its ability to improve the distribution of active metal and suppress carbon deposition. Interestingly, in this study, H$_2$ produced by all the synthesized catalysts was higher than CO in terms of yield.

Fig. 4(d) represents the profile of H$_2$:CO ratio during GDR at 973 K. Results show that the H$_2$:CO ratio of 15%Ni/EA catalyst was low (1.2–1.25), which can be ascribed to the accumulation of CO produced by the water gas shift reaction (WGS). The incorporation of Ru as promoter slightly reduced the H$_2$:CO ratio to about 1, suggesting that the incorporation of Ru could lessen the rate of reverse water gas shift (RWGS) reaction. A similar conclusion was reached by Chen et al. [59], who discovered that the H$_2$:CO ratio was approaching stoichiometric values when a promoter was used in conjunction with Ni/SiO$_2$ catalyst. In terms of H$_2$:CO ratio stability, 15%Ni/EA and 1%Ru-15%Ni/EA exhibited a declining trend, whereas the other catalysts exhibited a nearly stable trend over the course of the 8 h reaction. This trend correlates to the coke resistant nature of the catalyst. Moreover, space time yield (STY) in mmolg$_{cat}^{-1}$ min^{-1} for H$_2$ (STYH) and CO (STYCO) followed similar trend of reactant conversions; 3%Ru-15%Ni/EA (STYH = 7.1, STYCO = 6.9) > 4%Ru-15%Ni/EA (STYH = 6.5, STYCO = 6.3) > 5%Ru-15%Ni/EA (STYH = 5.9, STYCO = 5.3) > 2%Ru-15%Ni/EA (STYH = 5.5, STYCO = 5.6) > 1%Ru-15%Ni/EA (STYH = 5.3, STYCO = 5.5) > 15%Ni/EA (STYH = 5.1, STYCO = 4.9). The effective enhancement of the catalytic activity by the addition of Ru results from the positive changes in the properties of the catalyst, such as oxygen vacancies and metal dispersion. 3%Ru-15%Ni/EA had larger STY values compared to the other catalysts due to the small particle size and fine dispersion of

(a) **(b)**

(c)
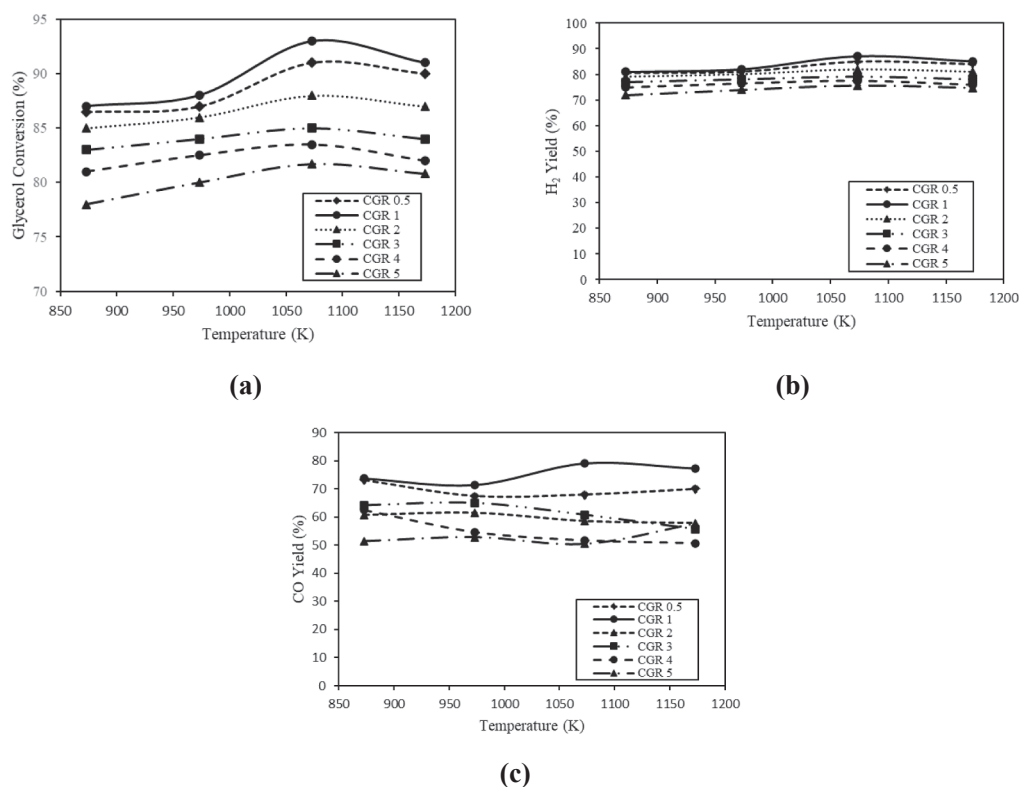
Fig. 5. Effect of reaction temperature at various CGR ratio on (a) glycerol conversion, (b) H_2 yield and (c) CO yield.

metal. Besides that, 3%Ru-15%Ni/EA had strong interaction between Ni and EA support as discussed in TPR and BET analyses.

In the representation of the catalytic performance of all the synthesized catalysts presented in Fig. 4, the utilization of 3%Ru promoter on 15%Ni/EA effectively enhanced the catalytic activity of Ni/EA due to the strong metal support interaction, well dispersion of Ni and smaller particle size. Furthermore, the 3%Ru-15%Ni/EA catalyst having high capacity to store or release oxygen proved beneficial for the gasification of carbon since the catalyst had the lowest rate of deactivation and carbon deposition.

3.2.2. Effect of reaction temperature

A study on the effect of reaction temperature at various CGR ratio ranging from 873 K to 1173 K was conducted using 3%Ru-15%Ni/EA. Fig. 5 represents the reactant conversion and products yield (H_2 and CO) in the order (i.e. highest to lowest) of CGR 1 > CGR 0.5 > CGR 2 > CGR 3 > CGR 4 > CGR 5. The results indicates that the best reaction temperature for GDR reaction using 3%Ru-15%Ni/EA was at 1073 K. At CGR of 1, the conversion obtained at 873 K, 973 K, 1073 K and 1173 K were 87%, 88%, 93% and 91% respectively. It was observed that although these differences are minimal, there is a direct relationship between temperature and glycerol conversion which is coherent with the Arrhenius characteristics. As the reaction temperature increased, the reactant conversion increased mainly due to the endothermic nature of GDR reaction. In addition, the slight differences observed in conversion as temperature increased is due to the dominance of various side reactions at different reaction temperatures. However, at 1173 K, the glycerol conversion slightly decreased because of the thermodynamically favored glycerol reforming as against the Boudouard reaction (BR) which is most likely to occur at high reaction temperature. This section will analyze in detail various side reactions (i.e., Boudouard reaction (BR) and reverse water gas shift (RWGS)) that drive the GDR reaction.

3.2.3. Water gas shift (WGS) reaction effects in relation to Temperature.

The WGS is an equilibrium process that occurs according to the stoichiometric reaction represented in Eq. (7). [60,61].

$$CO_{(g)} + H_2O_{(g)} \leftrightarrow CO_{2(g)} + H_{2(g)} \tag{7}$$

The forward reaction which is exothermic in nature converts CO and H_2O to H_2 and CO_2. The WGS is dominant at lower temperature range (below 973 K). At temperatures of 1073 K and 1173 K, the net WGS reaction is slow and negligible. Above 1473 K, the backward reaction which is the RWGS represented in Eq. (8) becomes dominant.

$$CO_{2(g)} + H_{2(g)} \leftrightarrow CO_{(g)} + H_2O_{(g)} \Delta H_{298K}^{\Delta} = 41 \; kjmol^{-1} \tag{8}$$
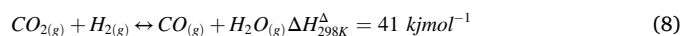
Therefore, in GDR reaction, to significantly minimize the effect of the WGS or RWGS reaction, the reaction should be conducted at 973–1173 K temperature range. This is to avoid the side reaction utilizing any valuable products such as CO at low temperatures (<973 K) or H_2 at higher temperatures (>1173 K). Furthermore, H_2O molecules from the glycerol cracking reacts with CO or incomplete oxidized carbon in WGS reaction to produce CO_2 and H_2, thereby shifting the product selectivity towards H_2 at lower reaction temperatures. The effect of the WGS reaction may not always be observed at temperatures between 973 K and 1073 K because of the presence of other catalytically dominant reactions such as glycerol cracking and GDR, which is the primary reaction. Also, the H_2 produced at lower temperature may take part in the complete reduction of the metallic catalyst during the GDR reaction. WGS reaction can also be affected by certain catalyst types. For instant, WGS reaction is fast on alkalized iron catalysts, but its effect is negligible on cobalt catalysts [62]. Though, it is essential to note that the WGS reaction is important in the analysis of chemical reaction that involves syngas. Amongst all the reactions involving syngas, the WGS reaction equilibrium is less sensitive to variation in temperature/temperature effects, hence, its equilibrium constant is least strongly dependent on temperature changes.
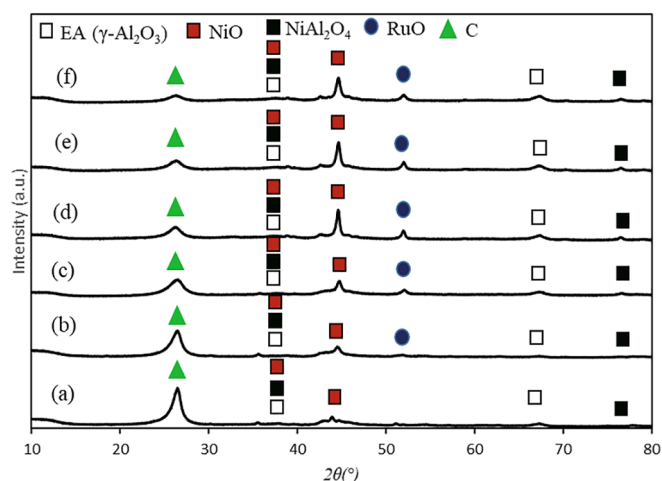
Fig. 6. XRD patterns of used (a) 15%Ni/EA, (b) 1%Ru-15%Ni/EA, (c) 2%Ru-1%Ru-15%Ni/EA, (d) 5%Ru-15%Ni/EA, (e) 4%Ru-15%Ni/EA and (f) 3%Ru-15%Ni/EA after 8 h GDR at T = 973 K, WHSV = 36 L $g_{cat}^{-1}h^{-1}$ and CGR of 1.

3.2.4. Boudouard reaction (BR) effects in relation to temperature

The BR referred to as the gasification of char is represented in Eq. (9). [63,64].

$$2CO_{(g)} \leftrightarrow CO_{2(g)} + C_{(S)} \Delta H^{â,°}{}_{298K} = -172 kjmol^{-1} \quad (9)$$
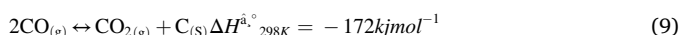
At low temperatures (<973 K), CO decomposes to C and CO_2 (i.e. BR). Due to the large enthalpy at this temperature, the equilibrium does not favor the formation of CO. However, when the entropy term starts to dominate and the free gibbs energy becomes negative, the reverse BR takes effect. At lower temperatures, the BR can be regarded as a principal source of carbon formation since the reaction is thermodynamically favored at these temperature, whereas at higher temperature, glycerol cracking is dominat and hence, the main source of carbon formation [65,66]. At high temperatures (>1273 K), almost all the available CO_2 reacts with C to form CO gas (reverse BR). When the reaction temperature is between 873 K and 1173 K, a significant amount of CO and CO_2 are present during the reaction. Furthermore, CO is naturally unstable which make it difficult to exist at lower temperature, hence it is easily oxidizes to CO_2. Therefore, when GDR reaction is carried out at 873–1173 K reaction temperature, the reaction has significant amount of CO_2 and CO due to the limiting effects of various side reactions. H_2:CO ratio > 1 indicates the occurrence of the BR or glycerol cracking where CO is used up, whereas H_2:CO ratio < 1 indicates the existence of RWGS

reaction where H_2 and CO_2 is consumed [66].

In this study, the increment in reactant conversion was majorly due to the endothermic nature of GDR reaction. 3%Ru-15%Ni/EA catalyst exhibited greater conversion of glycerol than other catalysts due to their greater coking resistance. However, at 1173 K, the conversion slightly decreased for all synthesized catalysts. This is due to the dominance of the thermodynamically favoured glycerol cracking reaction as opposed to the BR reaction, which is less likely to occur at high reaction temperatures [63 67].

3.3. Post reaction characterizations

The diffractogram for all the used catalysts after 8 h GDR reaction are shown in Fig. 6. All used catalysts revealed the presence of graphitic carbon at value 2θ = 26.69° (JCDPS card No. 75–0444) [68]. Interestingly, according to Fig. 6, the graphite X-ray reflection for all the promoted catalysts was reduced with the incorporation of Ru when compared to the 15% Ni/EA catalyst. This can be attributed to the high oxygen availability for the gasification of carbon in the promoted catalysts. The reduction in the intensity of the graphite peak was in the order of 15%Ni/EA > 1%Ru-15%Ni/EA > 2%Ru-15%Ni/EA > 5%Ru-15%Ni/EA > 4%Ru-15%Ni/EA > 3%Ru-15%Ni/EA indicating the superiority of 3%Ru-15%Ni/EA in inhibiting the formation of carbon. Meanwhile, the diffraction line recorded at 2θ = 38.25° and 44.82° corresponded to NiO (JCDPS card No. 01–073-1519). The existence of these peaks indicates the re-oxidation of Ni° by CO_2 during the GDR reaction. The intensity of spinel $NiAl_2O_4$ was observed at 2θ = 38.25°,

Table 2
Binding energies, atomic ratios and oxygen vacancies values obtained from the XPS analysis of all used catalysts.

Catalysts	Binding energy (eV)				Atomic ratio Ni/Al	Ov (%)
	2p3/2	2p3	C1s	O1s		
15%Ni/EA	856.0	870.0	284.5	531.0	0.15	24.5
1%Ru-15%Ni/EA	856.0	874.0	284.5	531.0	1.97	56.9
2%Ru-15%Ni/EA	855.5	873.5	284.5	531.5	2.14	62.4
3%Ru-15%Ni/EA	856.5	874.5	284.5	532.0	2.98	81.4
4%Ru-15%Ni/EA	855.5	874.0	284.5	531.0	2.74	78.7
5%Ru-15%Ni/EA	856.0	874.5	284.5	531.0	2.58	67.5

Fig. 7. Ni 2p XPS spectra of used promoted and unpromoted catalysts after 8 h GDR at T = 973 K, WHSV = 36 L gcat^{-1} h^{-1} and CGR of 1.
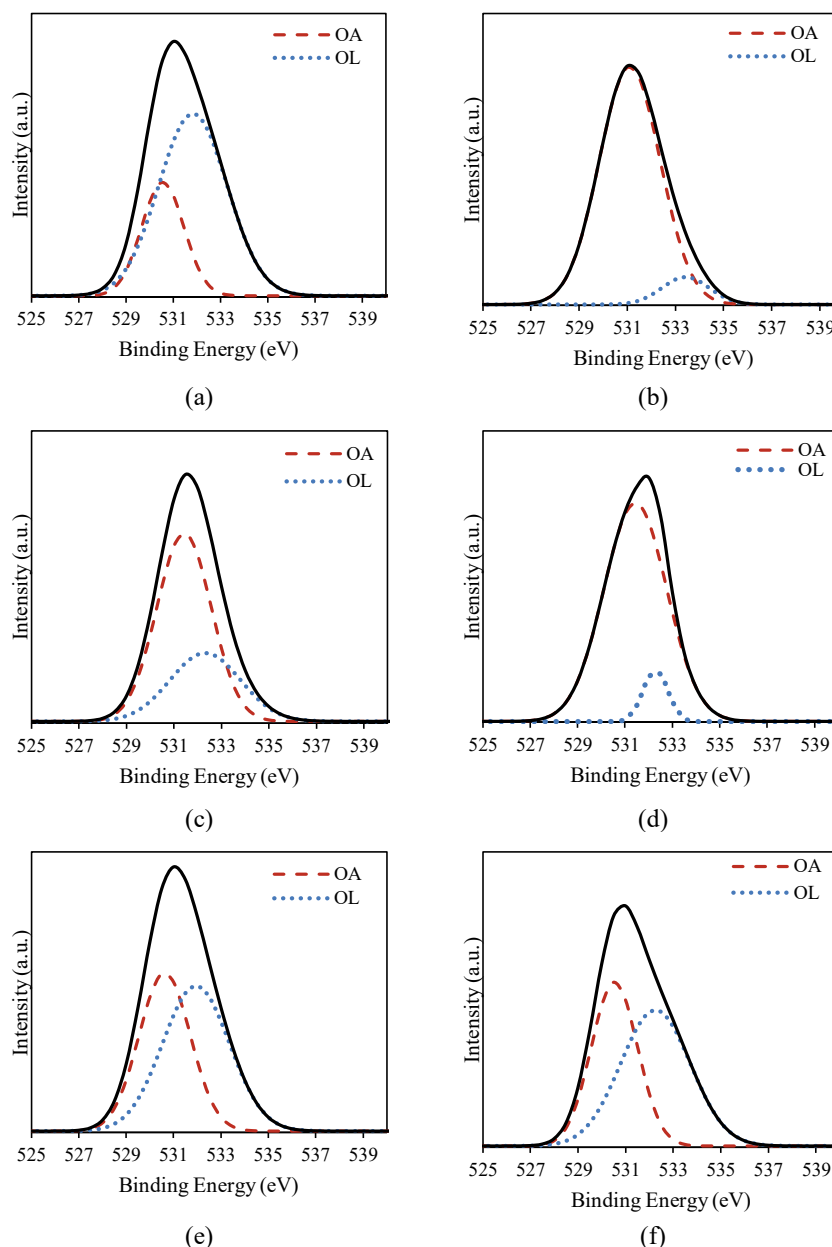
Fig. 8. O1s XPS spectra of used (a) 15%Ni/EA, (b) 1%Ru-15%Ni/EA, (c) 2%Ru-15%Ni/EA, (d) 3%Ru-15%Ni/EA, (e) 4%Ru-15%Ni/EA, (f) 5%Ru-15%Ni/EA catalysts after 8 h GDR at T = 973 K, WHSV = 36 L gcat^{-1}h^{-1} and CGR of 1.

77.54° (JCDPS card No: 00–010-0339) which is lower compared to spinel NiAl$_2$O$_4$ presented in Fig. 1.

XPS analysis was conducted to determine the atomic composition and oxidation state of the used unpromoted and promoted catalysts. Fig. 7 represents the XPS spectra measurement, and the calculated values of the binding energy (BE) are summarized in Table 2. As presented in Fig. 7, the Gaussian deconvolution peak of Ni 2p$_3$ spectra apperead for all used catalysts. There are two deconvoluted peaks located under Ni 2p3/2 region between 856.5 and 870.5 eV, which were attributed to NiO, Ni° and NiAl$_2$O$_4$ [56,57,58]. Two deconvualated peaks were also detected under Ni 2p$_3$ region at 793.5 –793.4 eV, 795.3 –795.5 eV and 796.6–796.9 eV which belonged to metallic Ni° and NiAl$_2$O$_4$. Meanwhile, peak at 803.1–803.2 eV represents NiO and satellite of Ni 2p$_3$ region [69,70]. The existence of Ni species was also consistent with the XRD findings as presented in Fig. 6. To investigate the effect of promoter on the dispersion of Ni over EA support, the atomic ratios of Ni/Al was calculated by XPS and summarized in Table 2.

The Ni/Al atomic ratios increased in the order: 15%Ni/EA (0.15%) < 1% Ru-15%Ni/EA (1.97%) < 2%Ru-15%Ni/EA (2.14%) < 5%Ru-15%Ni/ EA (2.58%) < 4%Ru-15%Ni/EA (2.74%) < 3%Ru-15%Ni/EA (2.88%). This trend is related to the enhanced dispersion of Ni with the incorporation of the Ru promoters. The enhancement in the atomic ratio of Ni/Al with the addition of promoter was also described by Meng et al. [71] to indicate a positive impact of promoter on the metal dispersion. The largest Ni/Al atomic ratios of 3%Ru-15%Ni/EA corroborates with the smaller particle size and strong Ni-EA interaction exhibited by the catalyst. This is in agreement with the findings from the BET and TPR analyses. These properties has resulted in superior performances of the 3%Ru-15%Ni/EA catalyst within 8 h of GDR compared to other catalysts.

Fig. 8 represent two main deconvolution peak of O 1s spectra as shown in Fig. 8 at BE of 527–533 eV and 527–537 eV. The first peak (i.e. 527–533 eV) represents lattice oxygen (O$_L$) which is related to Al$_2$O$_3$ and NiO. Meanwhile, the second peak (i.e. 527–537 eV) was ascribed to
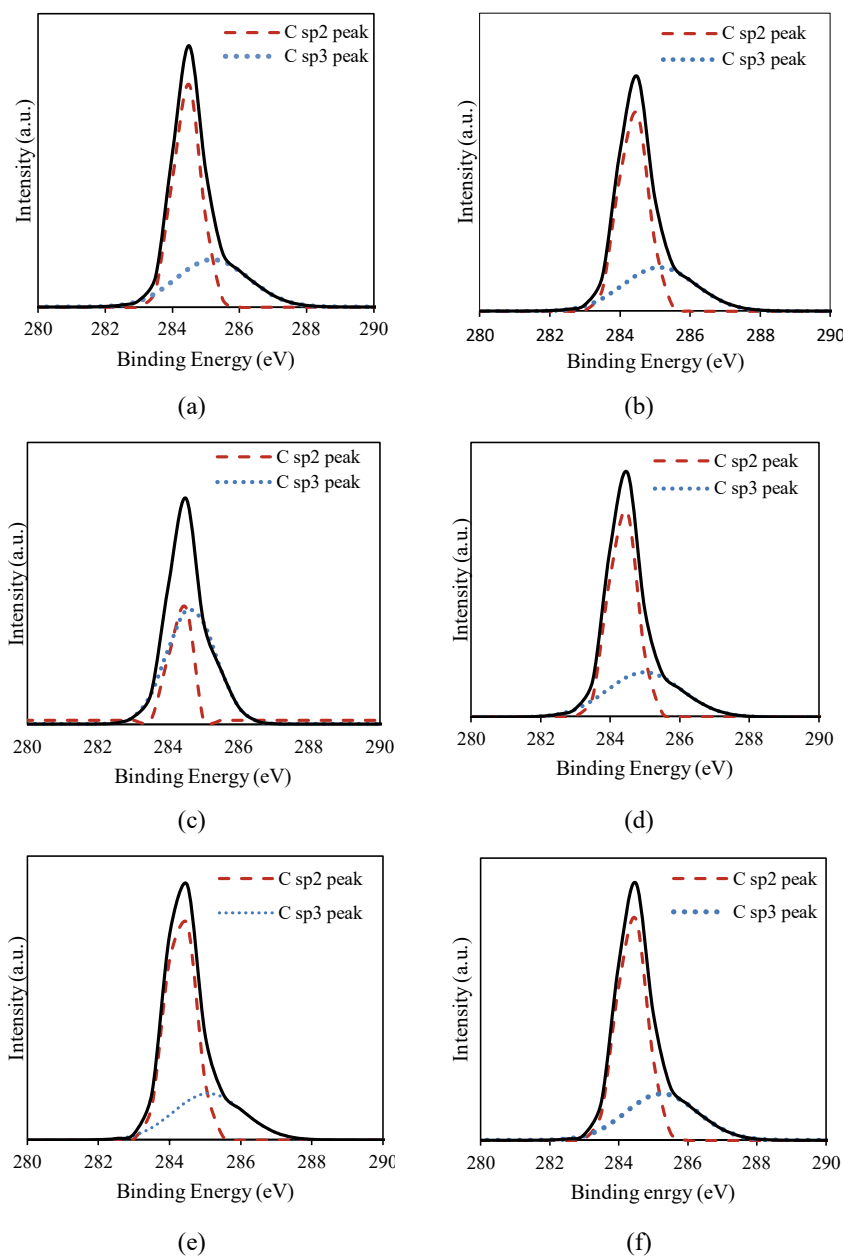
Fig. 9. C 1s XPS spectra of used (a) 15%Ni/EA, (b) 1%Ru-15%Ni/EA, (c) 2%Ru-15%Ni/EA, (d) 3%Ru-15%Ni/EA, (e) 4%Ru-15%Ni/EA, (f) 5%Ru-15%Ni/EA catalysts after 8 h GDR at T = 973 K, WHSV = 36 L $g_{cat}^{-1}h^{-1}$ and CGR of 1.

surface adsorbed oxygen (O_A) [72]. Previously, the number of oxygen vacancies (O_V) was calculated based on the peaks integrated area ratio for O_A and O_L (O_V (%) = (A_{OA}/(A_{OA} + A_{OL})) × 100(%)) [73]. As summarized in Table 2, 3%Ru-15%Ni/EA catalyst possesses the highest O_V of 81.4% followed by 4%Ru-15%Ni/EA, 5%Ru-15%Ni/EA, 2%Ru-15% Ni/EA, 1%Ru-15%Ni/EA and 15%Ni/EA. The high oxygen vacancies in 3%Ru-15%Ni/EA catalyst aided carbon gasification with the support (EA) acting as an active site to activate CO_2 during GDR reaction. This findings corroborated with the high catalytic activity and low rate of deactivation exhibited by 3%Ru-15%Ni/EA. As illustrated in Fig. 9, the spectra of C 1s of all the promoted catalysts represents the carbon species generated via BR. The curve at BE of 284.5 eV belonged to nonreactive and ordered graphitic carbon [74]. The structure of the carbon deposited using XPS analysis was in agreement with the TPO analyses. In addition, the spectra of C 1s for all the promoted catalysts indicated smaller peaks compared to the unpromoted 15%Ni/EA catalyst, which

further confirmed the Ru promoter's ability to resist carbon formation.

The total amount of carbon produced during 8 h GDR reaction was estimated through TPO analysis. From Fig. 10, peaks found around 800–1073 K represents the derivative weight profile which indicates the oxidation of carbon. According to Xin et al. [75], these peaks represent the removal of crystalline graphitic carbon during the reforming process. Based on literatures, the carbon species accumulates on the surface of the catalyst from the side reactions, either via CH_4 cracking (CH_4 = $2H_2$ + C(s)) or Boudouard (2CO = CO_2 + C(s)) [66,67]. Notably, the promoter incorporation significantly reduced the graphitic peak intensity. This result corroborates with the XRD analysis where the peak of graphite carbon reduced with the addition of the promoter (Fig. 6).

Furthermore, the percentage weight loss reduced with the incorporation of the promoter in the order of 15%Ni/EA (25.31%) > 1%Ru-15% Ni/EA (12.07%) > 2%Ru-15%Ni/EA (10.92%) > 5%Ru-15%Ni/EA (10.77%) > 4%Ru-15%Ni/EA (9.36%) > 3%Ru-15%Ni/EA (7.38%).
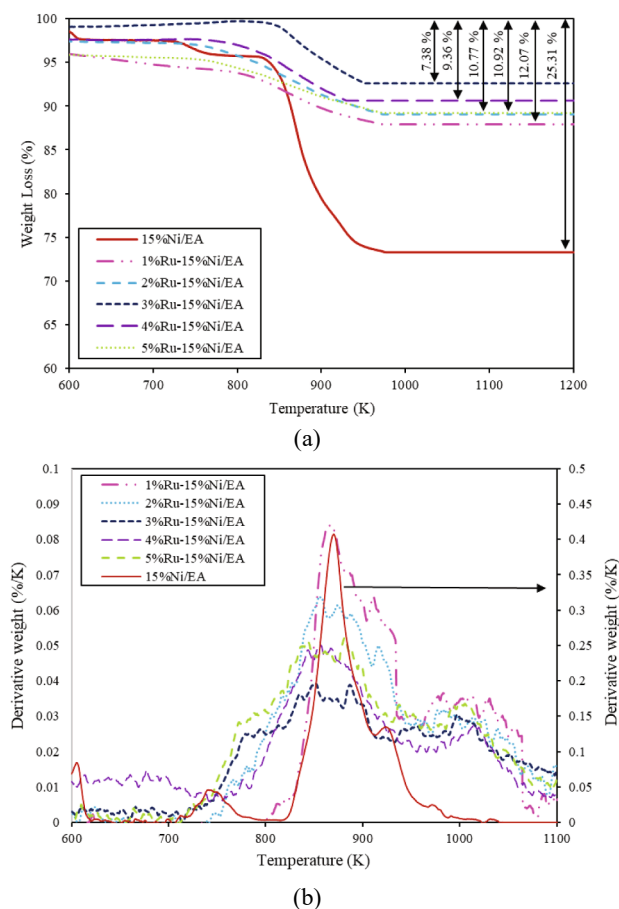
Fig. 10. TPO profile of the used (a) weght loss, (b) derivative weight catalysts after 8 h GDR at T = 973 K and CGR of 1.

The results revealed that Ru promoter reduced the deposition of carbon on the surface of catalyst during GDR reaction due to its multi-functional properties such as strong basic attributes and high oxygen vacancies. Interestingly, the trend from the percentage of weight loss and crystallite size was similar. According to Xin et al. [75], the increase in crystallite size promotes the carbon deposition rate. Therefore, this further verifies the small amount of carbon formation exhibited by 3%Ru-15%Ni/EA after 8 h GDR reaction.

The surface morphologies from TEM analysis of all used catalysts for GDR reaction are illustrated in Fig. 11. EA support presented as grey colour while Ni particles exist as dark dots. In the TEM image of the used 15%Ni/EA (cf. Fig. 11(b)), it can be seen that the is agglomeration of Ni metal particles, which results in larger Ni metal particle size (i.e. 6.23 nm). However, the Ni particle size was reduced in Fig. 11 (c)–(g) with less agglomeration, which indicates that the addition of Ru as promoter led to fine and narrow size distributions of Ni particles over EA support (cf. Table 1). Apparently, the crystallite size of the synthesized catalysts reduced in the order; 15%Ni/EA > 1%Ru-15%Ni/EA > 2%Ru-15%Ni/ EA > 5%Ru-15%Ni/EA > 4%Ru-15%Ni/EA > 3%Ru-15%Ni/EA, which directly relates to the metal support interaction of Ni and EA as discussed in TPR analysis. Therefore, strong Ni-EA interaction of the 3%Ru-15% Ni/EA catalyst showed superior sintering resistibility than the other catalysts. Also, 15%Ni/EA (i.e. Fig. 11 (b)) revealed the presence of a filamentous (FC) and graphitic (GC) type carbon. Usually, Ni-based catalyst used in reforming reactions lead to the formation of filamentous carbon [76,77]. Previous reports shows that this type of carbon can easily be gasified with CO_2 and thus does not give any negative impact on the catalytic activity in the reforming process [78]. However, this carbon could block the reactor faster and therefore limit the catalytic

activity. On the other hand, it is apparent that GC type carbon (as revealed by XRD analysis) was generated on the used catalysts (i.e. Fig. 11(c)-(g)). This type of carbon covers the metal and support surface thereby blocking reactants' accessibility to the catalyst's active sites, hence, restricting the reaction from occuring. Nevertheless, Ru are more carbon resistant than Ni, especially towards the formation of filamentous carbon [78]. This is due to the dissolution of carbon into the lattices of noble metals during the reaction, leaving the carbon species at the surface of the catalyst to be converted into CO or CO_2 [79].

3.4. Stability study

Catalytic performance of GDR for 15%Ni/EA and 3%Ru-15%Ni/EA catalysts was evaluated in a 72 h time-on-stream (TOS) under the given conditions (1 atm, stoichiometric feed ratio glycerol:CO_2 = 1:1, 1073 K). The study was conducted to examine the influence of promoter on the activity and stability of the 15%Ni/EA catalysts in the GDR reaction. Fig. 12 (a) showed that the promoted catalyst was stable during the 72 h TOS. As seen in Fig. 12 (a), a sharp drop was observed in the glycerol conversion, H$_2$ yield, and CO yield of the 15%Ni/EA catalyst with the percentage of deactivation about 9.3%. The glycerol conversion declined from about 56.7% to 49.1% after 30 h of reaction, and then the conversion became stable until 72 h. The formation of larger crystallites size or bulky NiO particles could be responsible for the distortion in accessibility to the active sites. The addition of Ru to the catalyst gave a superior catalytic activity and stability. For 3%Ru-15%Ni/EA catalyst, (i.e. Fig. 12 (b)) there was a slight drop in glycerol conversion from 95% to 92% after 6 h of reaction. The reactant conversion and product yield were stable after 6 h with the percentage of deactivation only about 2.2%. Similar findings were observed in the thermogravimetric studies for catalytic decomposition of methane using Ru-promoted Ni/Al$_2$O$_3$ catalyst [67]. The result revealed that the nucleation of graphitic carbon was observed for the initial induction period, which leads to increase in carbon formation. After reaching a plateau with respect to carbon content, the rate of carbon deposition begins to decline after a period of time. It has been suggested that the amount of carbon nucleation for a given catalyst depends mainly on the reaction temperature and gas-phase composition.

As shown in Fig. 12, the H$_2$:CO ratio was lower than two for both catalysts which is appropriate for downstream Fischer-Tropsch synthesis that can produce long-chain hydrocarbons. In addition, the Ru doped catalyst showed the highest product yield for H$_2$ and CO of about 86.1% and 76.7% respectively. The product yield decreased after 6 h TOS and exhibited similar behaviour with the product ratio and reactant conversion (see Fig. 12(a) and 10 (b)). Overall, incorporation of Ru as promoter enhanced the Ni-EA interaction and therefore improved the catalyst's stability at high reaction temperature for a longer reaction time.

4. Conclusions

The effectiveness of catalyst promoter (i.e. Ru) towards changing the physicochemical properties and catalytic activity of Ni/EA catalysts in GDR reaction was explored in this study. The promoter incorporation reduced both the pore diameter and BET surface area of Ni/EA to 16.5 nm and 125.32 m^2g^{-1} respectively. This can be attributed to improved dispersion of Ni particles on the EA surface and the reduction of the crystallite size of Ni which are situated on the pore and surface of the EA. In addition, H$_2$-TPR analysis showed that the small Ru crystallite size increased Ni-EA interaction. From the catalytic evaluation conducted, the reactants' conversion increased after the addition of Ru promoter to the Ni/EA catalyst in the order: 15%Ni/EA < 1%Ru-15%Ni/EA > 2%Ru-15%Ni/EA > 5%Ru-15%Ni/EA > 4%Ru-15%Ni/EA > 3%Ru-15%Ni/ EA. 3%Ru-15%Ni/EA possessed the highest values at about 93% glycerol conversion, 87% H$_2$ yield and 79% CO yield. The Ru promoter redox properties reduced the deactivation degree from 4.21% (15%Ni/EA) to
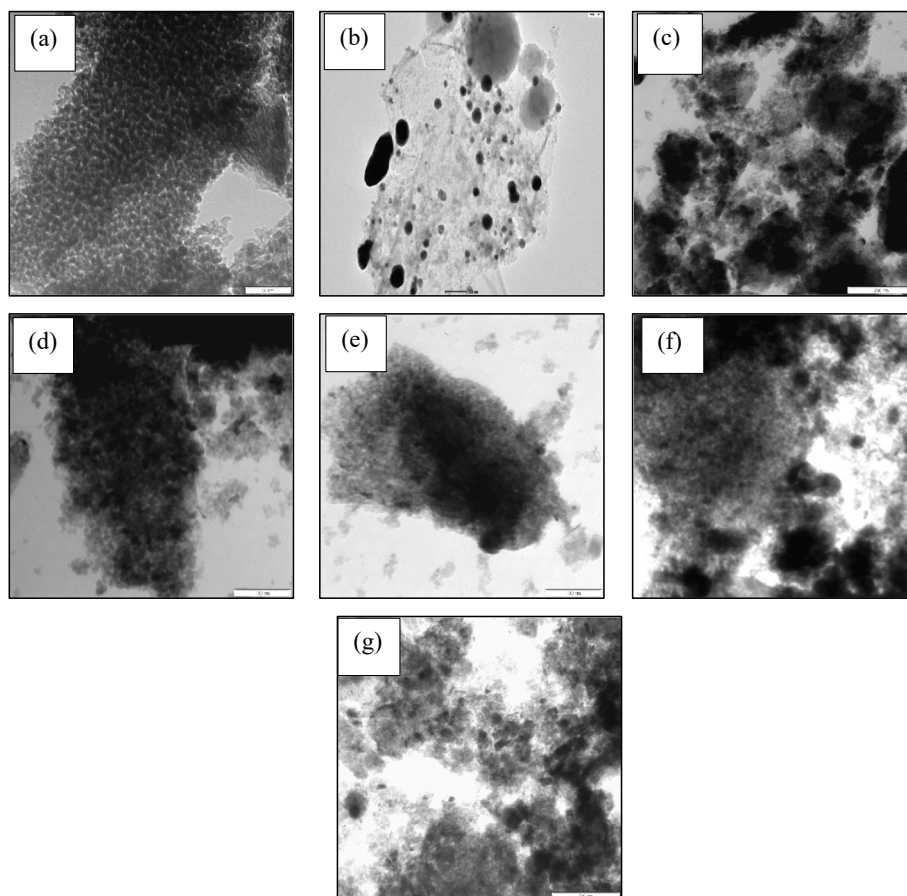
Fig. 11. TEM images of (a) EA support, (b), 15%Ni/EA, (c) 1%Ru-15%Ni/EA, (d) 2%Ru-15%Ni/EA, (e) 3%Ru-15%Ni/EA, (f) 4%Ru-15%Ni/EA, (g) 5%Ru-15%Ni/EA catalysts for 8 h of GDR reforming ay 973 K reaction temperature and CGR of 1.
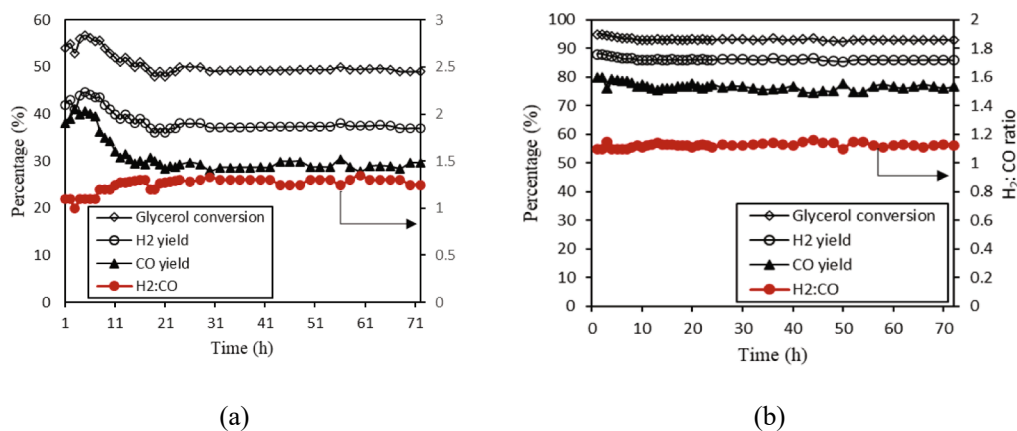
Fig. 12. TOS profile of glycerol conversion, H_2 yield and CO yield for 72 h, CGR of 1 and reaction temperature at 1073 K; (a) 15%Ni/EA; (b) 3%Ru-15%Ni/EA.

0.57% (3%Ru-15%Ni/EA). The highest Ni/Al atomic ratio for the 3%Ru-15%Ni/EA catalyst (2.88%) obtained from XPS analysis suggests the superior catalytic activity of 3%Ru-15%Ni/EA due to good dispersion of Ni compared to the other catalysts. The TPO results showed a decrease in the amount of carbon in the order of 15%Ni/EA > 1%Ru-15%Ni/EA > 2%Ru-15%Ni/EA > 4%Ru-15%Ni/EA > 5%Ru-15%Ni/EA > 3%Ru-15%Ni/EA. Therefore, 3%Ru-15%Ni/EA was able to effectively gasifiy carbon during the reaction and therefore enhanced the catalytic performance. In summary, excellent catalytic performance in GDR reaction was attained by 3%Ru-15%Ni/EA catalyst due to its high oxygen storage capability and excellent dispersion of Ni on EA support. This enhanced catalytic characteristics promoted carbon gasification and subsequently, increased the activity and stability towards H_2 and CO productions.

CRediT authorship contribution statement

Nurul Asmawati Roslan: Methodology, Formal analysis, Investigation, Writing – review & editing, Writing – original draft, Visualization, Data curation, Resources. **Sumaiya Zainal Abidin:** Conceptualization, Supervision, Project administration, Writing –

review & editing, Funding acquisition. **Osarieme Uyi Osazuwa:** Data curation, Writing – review & editing. **Chin Sim Yee:** Formal analysis, Resources. **Y.H. Taufiq-Yap:** Formal analysis.

Declaration of Competing Interest

The authors declare that they have no known competing financial interests or personal relationships that could have appeared to influence the work reported in this paper.

Acknowledgements

References

[1] Li X, Zhang L, Li Q, Zhang Z, Zhang S, Li Y, et al. Steam reforming of sugars: Roles of hydroxyl group and carbonyl group in coke formation. Fuel 2021;292:120282. https://doi.org/10.1016/j.fuel.2021.120282.

[2] Han K, Yu W, Xu L, Deng Z, Yu H, Wang F. Reducing carbon deposition and enhancing reaction stability by ceria for methane dry reforming over Ni@SiO$_2$@CeO$_2$ catalyst. Fuel 2021;291:120182. https://doi.org/10.1016/j.fuel.2021.120182.

[3] Arif NNM, Abidin SZ, Osazuwa OU, Vo N, Dai-Viet MT, Azizan Y-Y. Hydrogen production via CO$_2$ dry reforming of glycerol over Re-Ni/CaO catalysts. Int J Hydrogen. Energ 2019;44:20857–71.

[4] Wang X, Li M, Wang M, Wang H, Li S, Wang S, et al. Thermodynamic analysis of glycerol dry reforming for hydrogen and synthesis gas production. Fuel 2009;88:2148–53.

[5] Bac S, Say Z, Kocak Y, Ercan KE, Harfouche M, Ozensoy E, et al. Exceptionally active and stable catalysts for CO$_2$ reforming of glycerol to syngas. Appl Catal B-Environ 2019;256:117808.

[6] Bulutoglu PS, Say Z, Bac S, Ozensoy E, Avci AK. Dry reforming of glycerol over Rh-based ceria and zirconia catalysts: New insights on catalyst activity and stability. Appl Catal A- General 2018;564:157–71.

[7] Roslan NA, Abidin SZ, Ideris A, Dai-Viet NV. A review on glycerol reforming processes over Ni-based catalyst for hydrogen and syngas productions. Int J Hydrogen Energ 2020;45:18466–89.

[8] T. N. L. T. Ngo, K-Y. Chiang, C-F. Liu, Y-H. Chang, H-P. Wan. Hydrogen production enhancement using hot gas cleaning system combined with prepared Ni-based catalyst in biomass gasification. Int J Hydrogen Energ, 2020. *In Press.*.

[9] An S, Zhang Y, Hu X, Xie X, Wang Q, Chen H, et al. Durable Mn(II)Cr(III)Ox composites-supported Ni-based catalysts with wide dynamic range for hydrogen production via auto-thermal reforming of acetic acid. Fuel 2020;278:118227.

[10] Lima DS, Calgaro CO, Perez-Lopez OW. Hydrogen production by glycerol steam reforming over Ni based catalysts prepared by different methods. Biomass Bioenerg 2019;130:105358.

[11] Deng G, Zhang G, Zhu X, Guo Q, Liao X, Chen X, et al. Optimized Ni-based catalysts for methane reforming with O$_2$-containing CO$_2$. Appl Catal B-Environ 2021;289:120033.

[12] Jabbour K. Tuning combined steam and dry reforming of methane for "metgas" production: a thermodynamic approach and state-of-the-art catalysts. J Energy Chem 2020;48:54–91.

[13] Shafiee P, Alavi SM, Rezaei M. Mechanochemical synthesis method for the preparation of mesoporous Ni–Al$_2$O$_3$ catalysts for hydrogen purification via CO$_2$ methanation. J Energy Inst 2021;96:1–10.

[14] Ali S, Khader MM, Almarri MJ, Abdelmoneim AG. Ni-based nano-catalysts for the dry reforming of methane. Catal Today 2020;343:26–37.

[15] Chen F, Tao Y, Ling H, Zhou C, Liu Z, Huang J, et al. Ni-Cu bimetallic catalysts on Yttria-stabilized zirconia for hydrogen production from ethanol steam reforming. Fuel 2020;280:118612.

[16] de Araúje Moreira TG, de Carvalho Filho JFS, Carvalho Y, de Almeida JMAR, Romani PN, Sousa-Aguiar EF. Highly stable low noble metal content rhodium-based catalyst for the dry reforming of methane. Fuel 2021;287:119536.

[17] Larimi A, Khorasheh F. Renewable hydrogen production over Pt/Al$_2$O$_3$ nano-catalysts: Effect of M-promoting (M=Pd, Rh, Re, Ru, Ir, Cr). Int J Hydrogen Energ 2019;44:8243–51.

[18] Anil C, Modak JM, Madras G. Syngas production via CO$_2$ reforming of methane over noble metal (Ru, Pt, and Pd) doped LaAlO$_3$ perovskite catalyst. Molecular Catalysis 2020;484:110805.

[19] De Caprariis B, De Filippis P, Palma V, Petrullo A, Ricca A, Ruocco C, et al. Rh, Ru and Pt ternary perovskites type oxides BaZr(1–x)MexO$_3$ for methane dry reforming. Appl Catal A-General 2016;517:47–55.

[20] Khalighi R, Bahadoran F, Panjeshashi MH, Zamaniyah A, Tahouni N. High catalytic activity and stability of X/CoAl2O4 (X = Ni Co, Rh, Ru) catalysts with no observable coke formation applied in the autothermal dry reforming of methane lined on cordierite monolith reactors. Micropor Mesopor Mat 2020;305:110371.

[21] H. Zhou T. Zhang Z. Sui Y-An. Zhu, C. Han, K. Zhu, X. Zhou. A single source method to generate Ru-Ni-MgO catalysts for methane dry reforming and the kinetic effect of Ru on carbon deposition and gasification Appl Catal B-Environ 233 2018 143 159.

[22] Suzuki T, Iwanami H, Yoshinari T. Steam reforming of kerosene on Ru/Al$_2$O$_3$ catalyst to yield hydrogen. Int J Hydrogen Energ 2000;25:119–26.

[23] Li D, Nakagawa Y, Tomishige K. Methane reforming to synthesis gas over Ni catalysts modified with noble metals. Appl Catal A-General 2011;408:1–24.

[24] Ishihara A, Qian EW, Finahari IN, Sutrisna IP, Kabe T. Addition effect of ruthenium on nickel steam reforming catalysts. Fuel 2005;84:1462–8.

[25] Chen YG, Yamazaki O, Tomishige K, Fujimoto K. Noble metal promoted Ni$_{0.03}$Mg$_{0.97}$O solid solution catalysts for the reforming of CH$_4$ with CO$_2$. Catal Lett 1996;39:91–5.

[26] Jeong JH, Lee JW, Seo DJ, Seo Y, Yoon WL, Lee DK, et al. Ru-doped Ni catalysts effective for the steam reforming of methane without the pre-reduction treatment with H$_2$. Appl Catal A-Gen 2006;302:151–6.

[27] Basagiannis AC, Verykios XE. Influence of the carrier on steam reforming of acetic acid over Ru-based catalysts. Appl Catal B-Environ 2008;82:77–88.

[28] Wang M, Au C-T, Lai S-Y. H$_2$ production from catalytic steam reforming of n-propanol over ruthenium and ruthenium-nickel bimetallic catalysts supported on ceria-alumina oxides with different ceria loadings. Int J Hydrogen Energ 2015;40:13926–35.

[29] Lee J, Jang EJ, Kwak JH. Acid-base properties of Al$_2$O$_3$: Effects of morphology, crystalline phase, and additives. J Catal 2017;345:135–48.

[30] Son IH, Kwon S, Park JH, Lee SJ. High coke-resistance MgAl2O4 islands decorated catalyst with minimizing sintering in carbon dioxide reforming of methane. Nano Energy 2019;19:58–67.

[31] Papageridis KN, Siakavelas G, Charisiou ND, Avraam DG, Tzounis L, Kousi K, et al. Comparative study of Ni Co, Cu supported on γ-alumina catalysts for hydrogen production via the glycerol steam reforming reaction. Fuel Processing Technol 2016;152:156–75.

[32] Medeira RLBA, Figueredo GP, Macedo HP, Oliveira ĂAS, Rabelo-Neto RC, Melo DMA, et al. One-pot microwave-assisted combustion synthesis of Ni-Al$_2$O$_3$ nanocatalysts for hydrogen production via dry reforming of methane. Fuel 2021;287:119511.

[33] Barros BS, Melo DMA, Libs S, Kiennemann A. CO$_2$ reforming of methane over La$_2$NiO$_4$/α-Al$_2$O$_3$ prepared by microwave assisted self-combustion method. Appl Catal A-General 2010;378:69–75.

[34] Li B, Luo Y, Li B, Yuan X, Wang X. Catalytic performance of iron-promoted nickel-based ordered mesoporous alumina FeNiAl catalysts in dry reforming of methane. Fuel Process Technol 2019;193:348–60.

[35] Wang N, Chu W, Zhang T, Zhao XS. Synthesis, characterization and catalytic performances of Ce-SBA-15 supported nickel catalysts for methane dry reforming to hydrogen and syngas. Int J Hydrogen Energ 2012;37:19–30.

[36] Lee HC, Siew KW, Gimbun J, Cheng CK. Synthesis and characterisation of cement clinker-supported nickel catalyst for glycerol dry reforming. Chem Eng J 2014;255:245–56.

[37] Roslan NA, Abidin SZ, Osarieme UO, Yee CS, Taufiq-Yap YH. H$_2$-rich syngas from glycerol dry reforming over Ni-based catalysts supported on alumina from aluminum dross. Int J Hydrogen Energ 2021;46:309959–30975.

[38] How LF, Islam A, Jaafar MS, Taufiq-Yap YH. Extraction and Characterization of Γ-Alumina from Waste Aluminium Dross. Waste and Biomass Valori 2017;8:7–321.

[39] Yin M, He S, Yu Z, Wu K, Wang L, Sun C. Effect of alumina support on catalytic performance of Pt-Sn/Al$_2$O$_3$ catalysts in one-step synthesis of Nphenylbenzylamine from aniline and benzyl alcohol. Chinese J Catal 2013;34:1534–42.

[40] Paviotti MA, Faroldi BM, Cornaglia LM. Ni-based catalyst over rice husk-derived silica for the CO$_2$ methanation reaction: Effect of Ru addition. J Envirn Chem 2021;9:105173.

[41] M.Z. Hossain M.B.I. Chowdhury A.K. Jhawar P. A. Charpentier PA. Supercritical water gasification of glucose using bimetallic aerogel Ru-Ni-Al2O3 catalyst for H2 production Biomass and Bioenerg 107 2017 39 51.

[42] Smoljan CS, Crawford JM, Carreon MA. Mesoporous microspherical NiO catalysts for the deoxygenation of oleic acid. Catal Commun 2020;143:106046.

[43] Dieuzeide ML, Iannibelli V, Jobbagy M, Amadeo N. Steam reforming of glycerol over Ni/Mg/γ-Al$_2$O$_3$ catalysts. Effect of calcination temperatures. Int J Hydrogen. Energ 2012;37:14926–30.

[44] Siew KW, Lee HC, Gimbun J, Chin SY, Khan MR, Taufiq-Yap YH. Syngas production from glycerol-dry (CO$_2$) reforming over La-promoted Ni/Al$_2$O$_3$ catalyst. Renew Energ 2015;74:7–441.

[45] Ewbank JL, Kovarik L, Diallo FZ, Sievers C. Effect of metal–support interactions in Ni/Al$_2$O$_3$ catalysts with low metal loading for methane dry reforming. Appl Catal A-Gen 2015;494:57–67.

[46] Luisetto I, Sarno C, Felicis DD, Basoli F, Battocchio C, Tuti S, et al. Ni supported on γ-Al$_2$O$_3$ promoted by Ru for the dry reforming of methane in packed and monolithic reactors. Fuel Process Technol 2017;158:130–40.

[47] Jozwiak WK, Nowosielska M, Rynkowski J. Reforming of methane with carbon dioxide over supported bimetallic catalysts containing Ni and noble metal: I. Characterization and activity of SiO2 supported Ni-Rh catalysts. Appl Catal A-Gen 2005;280:233–44.

[48] Hossain MZ, Chowdhury MBI, Alsharari Q, Jhawar AK, Charpentier PA. Effect of mesoporosity of bimetallic Ni-Ru-Al2O3 catalysts for hydrogen production during supercritical water gasification of glucose. Fuel Process Technol 2017;159:55–6.

[49] Vasiliadou ES, Heracleous E, Vasalos IA, Lemonidou AA. Ru-based catalysts for glycerol hydrogenolysis—Effect of support and metal precursor. Appl Catal B-Environ 2009;92:90–9.

[50] Betancourt P, Rives A, Hubaut R, Scott CE, Goldwasser JA. A study of the ruthenium–alumina system. Appl Catal A-Gen 1998;170:307–14.

[51] Bossola F, Evangelisti C, Allieta M, Psaro R, Recchia S, Dal Santo V. Well-formed, size-controlled ruthenium nanoparticles active and stable for acetic acid steam reforming. Appl Catal B-Environ 2016;181:599–611.

[52] Li D, Li R, Lu M, Lin X, Zhan Y, Jiang L. Carbon dioxide reforming of methane over Ru catalysts supported on Mg-Al oxides: a highly dispersed and stable Ru/Mg(Al)O catalyst. Appl Catal B-Environ 2017;200:566–77.

[53] Wu HC, Chang YC, Wu JH, Lin LH, Lin IK, Chen CS. Methanation of CO_2 and reverse water gas shift reactions on Ni/SiO_2 catalysts: the influence of particle size on selectivity and reaction pathway. Catal Sci Technol 2015;5:4154–63.

[54] Andraos S, Abbas-Ghaleb R, Chlala D, Vita A, Italiano C, Laganà M, et al. Production of hydrogen by methane dry reforming over ruthenium-nickel based catalysts deposited on Al_2O_3, $MgAl_2O_4$, and YSZ. Int J Hydrogen Energ 2019;44 (47):25706–16.

[55] Dahdah E, Aouad S, Gennequin C, Estephane J, Nsouli B, Aboukaïs A, et al. Glycerol steam reforming over Ru-Mg-Al hydrotalcite-derived mixed oxides: Role of the preparation method in catalytic activity. Int J Hydrogen Energ 2018;43(43):19864–72.

[56] Pauletto G, Libretto N, Boffito DC, Miller JT, Jentys A, Patience GS, et al. Ni/CeO_2 promoted Ru and Pt supported on FeCrAl gauze for cycling methane catalytic partial oxidation—CPOX. Appl Catal B-Environ 2021;286:119849.

[57] Yang R, Xing C, Lv C, Shi L, Tsubaki N. Promotional effect of La_2O_3 and CeO_2 on $Ni/c-Al_2O_3$ catalysts for CO_2 reforming of CH_4. Appl Catal A-Gen 2010;385:92–100.

[58] Ibrahim AA, Umar A, Kumar R, Kim SH, Bumajdad A, Baskoutas S. Sm_2O_3-doped ZnO beech fern hierarchical structures for nitroaniline chemical sensor. Ceram Int 2016;42:16505–11.

[59] C. Chen X. Wang L. Zhang X. Zou W. Ding X. Lu X. Synthesis of mesoporous Ni-La2O3/SiO2 by ploy(ethylene glycol)-assisted sol-gel route as highly efficient catalysts for dry reforming of methane with a H2/CO ratio of unity Catal Comm 94 2017 38 41.

[60] Lee HC, Siew KW, Gimbun J, Cheng CK. Synthesis and characterisation of cement clinker-supported nickel catalyst for glycerol dry reforming. Chem Eng J 2014;255:56–245.

[61] Nabgan W, Mat R, Abdullah TAT, Nabgan B, Gambo Y, Zakaria ZY. Development of a kinetic model for hydrogen production from phenol over $Ni-Co/ZrO_2$ catalyst. J Enviro Chem 2016;4:52–4444.

[62] Schulz H. Comparing Fischer-Tropsch synthesis on iron- and cobalt catalysts. The dynamics of structure and function. Stud Surf Sci and Catal 2007;163:99–177.

[63] Fan MS, Abdullah AZ, Bhatia S. Catalytic technology for carbon dioxide reforming of methane to synthesis gas. ChemCatChem 2009;1:192–208.

[64] Wang S, Lu GQ, Millar GJ. Carbon Dioxide Reforming of Methane to Produce Synthesis Gas over Metal-Supported Catalysts: State of the Art. Energ Fuel 1996;10:896–904.

[65] Chen W, Zhao G, Xue Q, Chen L, Lu Y. High carbon-resistance $Ni/CeAlO_3-Al_2O_3$ catalyst for CH_4/CO_2 reforming. Appl Catal B-Environ 2013;136:136–7.

[66] Lovell EC, Horlyck J, Scott J, Amal R. Flame spray pyrolysis-designed silica/ceria-zirconia supports for the carbon dioxide reforming of methane. Appl Catal A-Gen 2017;546:47–57.

[67] Khajenoori M, Rezaei M, Meshkani F. Dry reforming over CeO_2-promoted Ni/MgO nano-catalyst: Effect of Ni loading and CH_4/CO_2 molar ratio. J Ind Eng Chemi 2015;21:22–717.

[68] Wang YF, Tsai CH, Chang WY, Kuo YM. Methane steam reforming for producing hydrogen in an atmospheric-pressure microwave plasma reactor. Int J Hydrogen Energ 2010;35:135–40.

[69] Arcotumapathy V, Vo DVN, Chesterfield D, Tin CT, Siahvashi A, Lucien FP, et al. Catalyst design for methane steam reforming. Appl Catal A-Gen 2014;479:87–102.

[70] Peck MA, Langell MA. Comparison of nanoscaled and bulk NiO structural and environmental characteristics by XRD, XAFS, and XPS. Chem Mater 2012;24(23):4483–90.

[71] Meng F, Li Z, Liu J, Cui X, Zheng H. Effect of promoter Ce on the structure and catalytic performance of Ni/Al_2O_3 catalyst for CO methanation in slurry-bed reactor. J Nat Gas Sci Eng 2015;23:250–8.

[72] Wang N, Shen K, Huang L, Yu X, Qian W, Chu W. Facile route for synthesizing ordered mesoporous Ni-Ce-Al oxide materials and their catalytic performance for methane dry reforming to hydrogen and syngas. ACS Catal 2013;3:1638–51.

[73] Zhang J, Li Y, Wang L, Zhang C, He H. Catalytic oxidation of formaldehyde over manganese oxides with different crystal structures. Catal Sci Techno 2015;5:2305–13.

[74] Dang MN, Ung TD, Phan HN, Truong QD, Bui TH, Phan MN, et al. A novel method for preparation of molybdenum disulfide/graphene composite. Mater Lett 2017;194:145–8.

[75] Xin J, Cui H, Cheng Z, Zhou Z. Bimetallic Ni-Co/SBA-15 catalysts prepared by urea co-precipitation for dry reforming of methane. Appl Catal A-Gen 2018;554:95–104.

[76] Kousi K, Chourdakis N, Matralis H, Kontarides D, Papadopoulu C, Verykios X. Glycerol steam reforming over modified Ni-based catalysts. Appl Catal A-Gen 2016;518:129–41.

[77] Nizah MFR, Taufiq-Yap YH, Rashid U, Teo SH, Nur ZAS, Islam A. Production of biodiesel from non-edible Jatropha curcas oil via transesterification using Bi_2O_3-La_2O_3 catalyst. Energ Convers Manage 2014;88:1257–62.

[78] K. Kousi D.I. Kondarides X.E. Verykios Papadopoulou. Glycerol steam reforming over modified Ru/Al2O3 catalysts Appl Catal A-Gen 542 2017 201 211.

[79] Papadopoulou C, Matralis H, Verykios X. Utilization of Biogas as a Renewable Carbon Source: Dry Reforming of Methane. In: Guczi L, Erdôhelyi A, editors. Catalysis for Alternative Energy Generation. New York, NY: Springer New York; 2012. p. 57–127. https://doi.org/10.1007/978-1-4614-0344-9_3.